ELSEVIER

Contents lists available at ScienceDirect

Electric Power Systems Research

journal homepage: www.elsevier.com/locate/epsr



Conditional Generative Adversarial Network-based framework for multi-feature uncertainty modeling in energy systems

Mojtaba Moradi-Sepahvand

Department of Wind Energy, Energy and Materials Transition Unit, TNO, The Netherlands

ARTICLE INFO

Keywords: Conditional Generative Adversarial Networks (cGAN) Hybrid power plants Scenario generation and reduction Stochastic optimization Uncertainty modeling

ABSTRACT

This paper presents a conditional Generative Adversarial Network (cGAN)-based framework for capturing uncertainty in the portfolio management of a hybrid power plant, with a particular focus on the joint variability of wind power output and electricity market prices. The proposed cGAN model generates realistic scenarios for multiple correlated feature vectors simultaneously, while preserving both temporal dependencies and interfeature correlations. A large set of scenarios is produced and subsequently reduced to a limited number of representative scenarios using a clustering technique that retains the statistical structure and correlations among variables. These representative scenarios are then integrated into a developed stochastic Mixed-Integer Linear Programming (MILP) model within the EMERGE platform at TNO to optimize hybrid power plant portfolio management under uncertainty. Results based on multi-year data demonstrate that the approach reduces imbalance costs from 20.63% to 14.94% compared to a deterministic baseline that relies only on point forecasts, which highlights the effectiveness of the proposed framework in enhancing operational robustness and market alignment.

1. Introduction

1.1. Background and literature review

The increasing penetration of renewable energy sources, such as wind and solar, has significantly transformed the operational landscape of modern power systems. Hybrid power plants (HPPs), which integrate multiple energy assets such as wind farms, solar PV, energy storage, and Power-to-X technologies, offer enhanced flexibility and reliability. However, these systems also introduce high levels of operational uncertainty due to the variability of renewable output and fluctuations in electricity market prices. Accurate modeling of such uncertainties is essential for effective portfolio management, particularly when deviations from forecasts can lead to significant imbalance costs. Scenario-based stochastic optimization has emerged as a widely used technique to manage these uncertainties [1]. Traditional methods rely on statistical approaches such as Monte Carlo or copula-based sampling [2], which often fall short in capturing nonlinear dependencies, multi-feature interactions, and temporal correlations, especially when dealing with joint uncertainty in wind power and market prices. In [3], the distribution of unknown variables is modeled using the copulabased approach, and Monte Carlo is then utilized to produce wind scenarios. [4] develops the autoregressive moving average (ARMA) model for wind scenarios. The uncertainty of wind forecast error is

examined using empirical distributions in [5], and to create wind scenarios, the distributions are sampled using an inverse transform sampling technique. Using historical data, the majority of these traditional scenario generation techniques first match the parameters of a presumptive statistical distribution model before creating scenarios through sampling from the distribution model. However, as the assumptions might not hold in practice, particularly for operational scenarios involving multivariate uncertain variables, it is difficult to derive reliable statistical assumptions of uncertain variables and to fit the corresponding parameters. Furthermore, it can be challenging to sample from complex distributions [4]. As a result, the scalability and applicability of these statistical model-based methods in downstream decision-making tasks remain limited [1].

Recent advances in deep-learning based generative models, particularly Generative Adversarial Networks (GANs), have shown promising capabilities in high-dimensional scenario generation without the need for explicit probabilistic assumptions. Instead of directly optimizing the maximum likelihood function, GAN tackles the problem by alternately training two deep neural networks, the generator and the discriminator [1]. It was first used in [6] for generating renewable energy scenarios which demonstrated that GANs can efficiently produce a wide range of diverse scenarios in this context. GAN performance is improved in order to generate better scenarios with focus on solving

E-mail address: mojtaba.moradisepahvand@tno.nl.

Nomenclature of Hybrid Power Plant Optimization

Indices and Sets:

t, s	Time interval and scenario indices, $t \in \mathcal{T}$,
	$s \in S$

Parameters:

β , α	Risk aversion ($0 \le \beta \le 1$), CVaR confidence
	level (95%)
p_s , M , SOC^{init}	Probability of scenarios, Big-M, Initial
	battery state-of-charge [MWh]
$\lambda_{t,s}, \lambda_t^{h2}$	Electricity price [€/MWh], hydrogen price
	[€/kg]
$c^{\mathrm{su}}, c^{\mathrm{h}2}$	Electrolyzer startup cost [€], hydrogen
	production cost [€/kg]
$\eta^{\mathrm{ch}}, \eta^{\mathrm{dis}}, c^{\mathrm{b}}$	Battery charge/discharge efficiency and
	operational costs [€/MWh]
$P_{t,s}^{\text{w,scn}}, P_{t,s}^{\text{pv,scn}}$	Scenario values of wind and PV power
$P^{[\cdot],\max}$	Rated capacity of asset
	$[\cdot] \in \{w, pv, h2, com, b, g\}, \text{ which denotes}$
	wind farm, photovoltaic units, electrolyzer
	hydrogen compressor, battery energy
	storage (ch/dis), and grid connection,
	respectively
c^{su} , c^{h2} η^{ch} , η^{dis} , c^{b} $P_{t,s}^{\text{w,scn}}$, $P_{t,s}^{\text{pv,scn}}$	[€/kg] Electrolyzer startup cost [€], hydrogen production cost [€/kg] Battery charge/discharge efficiency and operational costs [€/MWh] Scenario values of wind and PV power Rated capacity of asset [·] ∈ {w, pv, h2, com, b, g}, which denote wind farm, photovoltaic units, electrolyze hydrogen compressor, battery energy storage (ch/dis), and grid connection,

Decision Variables:

$R_{t,s}^{[\cdot]}, C_{t,s}^{[\cdot]}$ $P_{t,s}^{[\cdot]}, S_{t,s}^{[\cdot]}$	Revenue and cost of asset $[\cdot]$ at t, s $[\in]$
$P_{t,s}^{[\cdot]}, S_{t,s}^{[\cdot]}$	Power [MW] and setpoint variable of asset
-,-	$[\cdot]$ at $t, s \ (0 \le S_{t,s}^{[\cdot]} \le 1)$
$U_{t,s}^{\mathrm{b}}, U_{t,s}^{\mathrm{g}}$	Binary variables for charging/discharging,
-,,	and import/export status
$SOC_{t,s}^{b}$, $CVaR_{\alpha}$	Battery state of charge [MWh], Conditional
-,-	Value-at-Risk at α [€]
$H_{t,s}^{\mathrm{p}}, H_{t,s}^{\mathrm{deliv}} \ Z_{t,s}^{\mathrm{su}}$	Total Produced and delivered hydrogen [kg]
$Z_{t,s}^{\mathrm{su}}$	Binary variables of electrolyzer startup
Π_s , Ψ_s	Total profit and CVaR slack variable at
	scenario $s \in [$

model overfitting issue discriminator regularization in [7]. GAN-based scenario generation is implemented to stochastic optimal scheduling problem in [8]. Conditional GANs (cGANs), which incorporate auxiliary input (e.g., time indices or forecasts), enable structured scenario generation with control over temporal evolution and external features [9, 10]. However, standard GAN architectures still struggle to capture the dynamic dependencies and joint distributions of time-series data relevant to energy systems. To overcome these limitations, several works have introduced time-series-specific GAN architectures. For instance, an Informer-TimeGAN hybrid model is proposed in [11] that combines temporal convolutional networks with self-attention mechanisms for day-ahead wind power scenario generation. That model integrates auxiliary classification loss and seasonal embedding to enhance scenario diversity and accuracy. Similarly, [12] developed a Progressive Growing of GAN (PG-GAN) and multi-objective optimization framework for wind power scenario generation, aiming to balance trade-offs between statistical similarity and forecast diversity. In [13], Conditional Style-based GANs are used to control scenario generation by injecting style features into latent spaces to preserve variability while ensuring statistical realism. GAN-based generation is extended in [14] to integrated energy systems, addressing operational constraints and data sparsity through a joint forecasting-scenario framework. A comprehensive review of uncertainty handling in renewable energy applications is provided in [1], covering stochastic optimization approaches, uncertainty modeling methods, scenario generation techniques, and their respective advantages, limitations, and future research directions.

1.2. Research gaps and contributions

Despite recent progress, the application of conditional GANs for *joint* multi-feature uncertainty modeling in HPP portfolio management remains limited. Accurately capturing the temporal dynamics and cross-feature dependencies between wind generation and electricity prices is critical for improving dispatch decisions and market participation. Furthermore, integrating such high-fidelity scenarios into a tractable stochastic optimization framework demands robust scenario reduction techniques that retain essential correlations while minimizing computational burden.

To address these challenges, this paper presents a novel framework that extends the conditional GAN approach to jointly model the uncertainty in wind power output and electricity market prices for HPP portfolio optimization. The proposed model incorporates a Transformer-GRU hybrid architecture designed to capture both temporal dependencies and cross-feature correlations that are critical in power system applications. While conventional cGAN implementations are typically used as standalone scenario generators, the approach of this paper directly integrates the cGAN-generated scenarios into a stochastic optimization framework for optimal HPP dispatch. This enables the creation of realistic hourly day-ahead scenarios that are both computationally tractable and operationally relevant. To reduce complexity while preserving statistical fidelity, a clustering-based scenario reduction method is employed. The resulting representative scenarios, along with their associated probabilities, are embedded into a stochastic Mixed-Integer Linear Programming (MILP) formulation within the EMERGE platform at TNO [15], supporting robust decision-making under uncertainty.

The key contributions of this work are summarized as follows:

- (i) A unified cGAN-based framework is developed for the joint generation of realistic day-ahead scenarios of wind power and electricity prices. The model integrates a Transformer–GRU architecture to capture both temporal dependencies and inter-feature correlations, and employs a clustering-based scenario reduction technique to ensure statistical representativeness while maintaining computational tractability;
- (ii) The reduced scenario set, together with associated probabilities, is integrated into a stochastic MILP optimization model within the EMERGE platform at TNO [15]. The complete framework is validated using multi-year data from the Netherlands, demonstrating tangible improvements in hybrid power plant scheduling and imbalance cost reduction relative to a deterministic forecast-based baseline.

1.3. Paper structure

The remainder of this paper is structured as follows. Section 2 describes the proposed cGAN-based scenario generation and reduction methodology. Section 3 outlines the case study design, data, and parameters. Section 4 presents the optimization results and performance comparison. Finally, Section 5 concludes with key insights and future research directions.

2. Methodology

Power system datasets often exhibit strong temporal dependencies, seasonal patterns, and high correlations between electricity prices and renewable generation. To address these characteristics, the proposed framework employs a Transformer–GRU hybrid generator to capture both long- and short-term dynamics while preserving cross-variable relationships. This section then outlines the overall structure of the proposed cGAN method, starting with data preprocessing for model training, followed by the cGAN architecture and training Strategy.

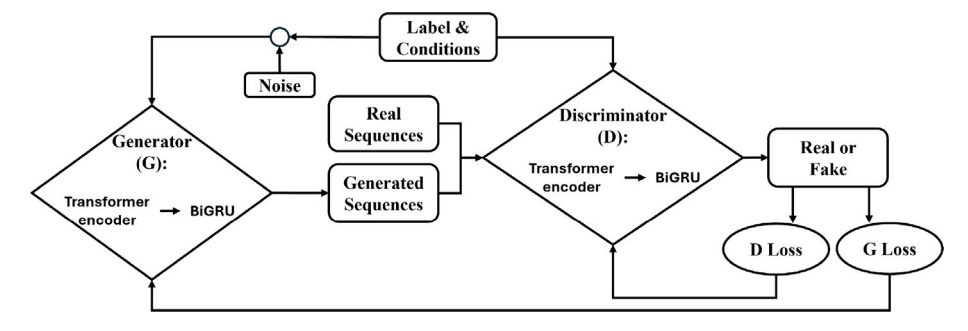


Fig. 1. Architecture of the proposed cGAN, where both generator and discriminator use a Transformer-BiGRU core with final dense layers producing multi-feature outputs (generator) or authenticity logits (discriminator).

2.1. Data loading and preprocessing

The dataset consists of hourly time series data for wind power output, electricity market prices, and forecasts for wind generation, market prices, load, and solar generation. We utilize z-score normalization to standardize these features, ensuring that they have a mean of zero and a standard deviation of one. This is crucial for the effective training of the cGAN model. We generate hourly labels (0 to 23) to preserve the intraday structure. The standardized data is then reshaped into daily sequences of size (24×7) , representing 24 time steps across seven dimensions, one label, two target features, and four conditioning inputs. From the multi-year dataset, the last four days are reserved as the test set, while the remaining historical data is split into training (80%) and validation (20%) subsets. This processed dataset serves as the input for the cGAN described in the following subsection.

2.2. cGAN architecture and training strategy

The developed cGAN generates realistic multi-feature time series conditioned on external inputs. The architecture combines Transformer encoders, which capture long-range dependencies through self-attention mechanisms [16–18], with Gated Recurrent Units (GRUs), which efficiently model temporal dynamics in sequential data [19,20].

2.2.1. cGAN architecture

As shown in Fig. 1, the proposed cGAN adopts a hybrid architecture in both generator and discriminator. Each network processes the input sequence through a Transformer encoder, capturing global inter-variable dependencies via self-attention with sinusoidal positional encoding, followed by a bidirectional GRU (BiGRU) [21] to model forward and backward temporal dynamics. This Transformer-BiGRU sequence enables learning of both long-range contextual relationships and local temporal patterns. The generator's output layers map these representations to multi-feature sequences, while the discriminator produces per-time-step logits indicating authenticity. This combination yields synthetic sequences that are realistic and context-aware.

Generator The generator maps a random noise vector $z \in \mathbb{R}^d$ and auxiliary conditions to 24-hour sequences of multiple target features (e.g., wind power, electricity price). Conditional inputs, including forecasted variables and hourly labels, are processed through spectral-normalized dense layers and embedded to preserve temporal semantics. The noise vector is broadcast across the time dimension and concatenated with the embedded inputs, then projected to a latent space. A Transformer encoder with sinusoidal positional encoding captures global temporal dependencies, followed by a BiGRU to model sequential dynamics in both directions. Time-distributed dense layers with Swish activations and spectral normalization refine the representation, and a final dense layer outputs the synthetic sequence for each time step.

Discriminator The discriminator functions as a binary classifier, distinguishing real from synthetic sequences while conditioned on the same inputs (hourly labels and forecasted features). Real and generated sequences are embedded with their conditional information, processed through spectral-normalized dense layers, and concatenated before projection. The sequence passes through a Transformer encoder with sinusoidal positional encoding and a BiGRU to capture temporal dependencies in both directions. Time-distributed dense layers with spectral normalization and LeakyReLU activations refine the features, and a final dense layer outputs scalar logits per time step which represents the probability of each slice being real. During adversarial training, the discriminator becomes better at telling real and synthetic sequences apart, while the generator simultaneously learns to fool it. This ongoing competition gradually pushes the generator to produce sequences that are increasingly realistic and temporally coherent.

2.2.2. Training strategy

The model is trained using mini-batch stochastic optimization (e.g., 64 sequences per batch) with the Adam optimizer [22], allowing it to efficiently learn from the full dataset over multiple epochs. It follows a hybrid approach that blends adversarial, feature matching, and reconstruction losses, while the Wasserstein GAN with Gradient Penalty (WGAN-GP) framework [23,24] is applied to guarantee stable and reliable convergence.

Loss functions To stabilize training and avoid mode collapse, we adopt the WGAN-GP [23,24]. The discriminator is trained to assign higher scores to real samples and lower scores to generated (fake) ones. The loss function for the discriminator is defined as:

$$\mathcal{L}_D = \mathbb{E}_{\hat{x} \sim \mathbb{P}_q}[D(\hat{x})] - \mathbb{E}_{x \sim \mathbb{P}_r}[D(x)] + \lambda_{gp} \cdot \mathsf{GP}(x, \hat{x})$$
 (1)

where $x \sim \mathbb{P}_r$ and $\hat{x} \sim \mathbb{P}_g$ denote samples from the real and generated data distributions, respectively. In practice, these expectations are computed over mini-batches of real and synthetic sequences. The discriminator $D(\cdot)$ outputs a scalar score indicating sample realism. The gradient penalty term $GP(x,\hat{x})$ is computed using interpolated pairs of real and fake data within each batch. λ_{gp} is a regularization coefficient controlling the strength of the gradient penalty term.

The generator is trained to produce realistic sequences that not only deceive the discriminator but also retain structural similarity to real data. To achieve this, a composite loss function consisting of three components is defined:

$$\mathcal{L}_{G} = \lambda_{adv} \cdot \mathcal{L}_{adv} + \lambda_{fm} \cdot \mathcal{L}_{fm} + \lambda_{recon} \cdot \mathcal{L}_{recon}$$
(2)

where

- $\mathcal{L}_{adv} = \mathbb{E}_{\hat{x} \sim \mathbb{P}_g} \left[\log D(\hat{x}) \right]$ is the adversarial loss, which encourages the generator to produce sequences that the discriminator classifies as real.
- $\mathcal{L}_{fm} = \|f(x) f(\hat{x})\|_2^2$ is the *feature matching loss*, which minimizes the distance between intermediate activations $f(\cdot)$ of the discriminator on real (x) and generated (\hat{x}) data.

• $\mathcal{L}_{recon} = \|x - \hat{x}\|_2^2$ is the *reconstruction loss*, measured as the mean squared error (MSE) between real and generated sequences.

The weights λ_{adv} , λ_{fm} , and λ_{recon} control the relative contribution of each term and are tuned via hyperparameter optimization.

Optimization The generator and discriminator are optimized using the Adam algorithm with learning rate decay [22]:

$$\eta_t = \eta_0 \cdot \gamma^{\lfloor t/T \rfloor} \tag{3}$$

where η_0 is the initial learning rate, γ is the decay rate, T is the decay step interval, and t is the training iteration. The loss functions for the discriminator (\mathcal{L}_D) and generator (\mathcal{L}_G) follow the WGAN-GP formulation, with generator loss combining adversarial, feature matching, and reconstruction components. Hyperparameters, including latent dimension, learning rates, and batch size, are tuned using Bayesian optimization via Optuna [25].

Optimization The generator and discriminator are optimized using the Adam algorithm with learning rate decay [22]:

$$\eta_t = \eta_0 \cdot \gamma^{\lfloor t/T \rfloor} \tag{4}$$

where η_0 is the initial learning rate, γ is the decay rate, T is the decay step interval, and t is the training iteration.

The loss functions for the discriminator (\mathcal{L}_D) and generator (\mathcal{L}_G) follow the WGAN-GP formulation, with the generator loss combining adversarial, feature matching, and reconstruction components.

Hyperparameters such as latent dimension, generator and discriminator learning rates, and batch size are optimized through Bayesian search using Optuna [25]. The objective function evaluates different configurations by training the model for a small number of epochs and selecting the best setting based on a composite validation metric explained in the next part. Specifically, each Optuna trial suggests candidate values for the key hyperparameters and initializes a GAN instance accordingly. After a few training epochs, the trial computes validation performance, and the composite metric in (8) is used to guide the selection of optimal parameters. The best trial yields the final values used in full training.

Validation and evaluation Model performance is evaluated after each epoch based on:

• Normalized RMSE between real (x) and generated (\hat{x}) data [26]:

$$nRMSE(x, \hat{x}) = \frac{\sqrt{\frac{1}{n} \sum_{i=1}^{n} (x_i - \hat{x}_i)^2}}{\max(x) - \min(x)}$$
 (5)

• *R*² *score* to measures how well the generated values explain the variance in the real data [27]:

$$R^{2} = 1 - \frac{\sum_{i=1}^{n} (x_{i} - \hat{x}_{i})^{2}}{\sum_{i=1}^{n} (x_{i} - \bar{x})^{2}}$$
 (6)

where \bar{x} is the average of all x_i .

• *KDE overlap* between the empirical distributions of real and synthetic data, computed as [28]:

$$KDE = \int \min \left[\hat{f}_x(u), \hat{f}_{\hat{x}}(u) \right] du$$
 (7)

where \hat{f}_x and $\hat{f}_{\hat{x}}$ are the kernel density estimators.

A composite validation metric is computed to jointly assess accuracy and statistical fidelity:

$$\mathcal{M} = c_1 \cdot \text{nRMSE} - c_2 \cdot \text{KDE} - c_3 \cdot R^2$$
 (8)

where c_1 , c_2 , and c_3 are weighting coefficients that balance the tradeoffs between reconstruction error (nRMSE), distributional similarity (KDE overlap), and explained variance (R^2 score). The generator model achieving the lowest exponentially smoothed value of $\mathcal M$ during training is selected as the final model.

```
Algorithm 1 Training Procedure for the Proposed cGAN Model
```

```
Require: Preprocessed training and validation datasets
Require: Generator G, Discriminator D, and hyperparameters \theta
 1: Initialize G and D with \theta, including learning rate schedules
 2: for each epoch do
 3:
       for each batch in training set do
 4:
           Sample noise vector z \sim \mathcal{N}(0, I)
           Generate synthetic data \hat{x} = G(z, \ell, \text{conditions})
 5:
           for k steps do
 6:
 7:
               Compute \mathcal{L}_D and \mathcal{L}_G and update G and D using gradient
    descent
           end for
 8:
       end for
 9:
       Evaluate on validation set using the composite validation metric
10:
    of (8)
11:
       Update best generator if the composite metric improves
12:
       if no improvement for P epochs then
           Reduce learning rates considering (4) and (9)
13:
14:
           if no improvement for P + \delta epochs then
15:
               Reload best generator weights
16:
           end if
        end if
17:
18: end for
19: Load best generator weights for final inference and scenario
```

Adaptive training and early stopping Building upon the decaying learning rate strategy used in the optimization phase (4), adaptive training mechanisms are employed to further improve model robustness. Specifically, if the composite validation metric $\mathcal M$ does not improve for a predefined patience window P, the learning rates of both the generator and discriminator are reduced. If stagnation persists for an additional δ epochs, the generator is rolled back to the best-performing state. The learning rate update rule is:

generation

$$\eta_t \leftarrow \max(\eta_t \cdot \lambda^D, \eta_{\min}),$$
(9)

where $\lambda^D < 1$ is the decay factor, and η_{\min} is the minimum learning rate threshold to maintain training stability.

A high-level overview of the training procedure for the proposed cGAN framework is presented in Algorithm 1. The algorithm outlines the key stages including stochastic data generation, loss evaluation, gradient-based updates, and validation monitoring using composite performance metrics.

Scenario generation & reduction To capture the stochastic nature of wind generation and electricity market prices, a large set of synthetic day-ahead scenarios is produced using the trained cGAN generator. For each test day, the generator receives a latent noise vector $z^{(i)}$, hourly time labels \mathcal{E}_{t} , and standardized forecasted features as the conditions. It then outputs a 24-hour sequence of synthetic values representing both wind power and market prices:

$$\hat{x}_t^{(i)} = G(z^{(i)}, \ell_t, conditions_t), \quad i = 1, \dots, N,$$
(10)

where $G(\cdot)$ denotes the generator and N is the total number of generated scenarios. Each scenario $\hat{x}_t^{(i)}$ represents a possible realization of joint wind-price evolution over a 24-hour horizon. The generated sequences are denormalized to the original scale using the training data statistics and stored in matrices of shape $[N \times 24]$ for both price and wind features.

To reduce computational complexity in downstream stochastic optimization models, the set of N raw scenarios is clustered using K-Means clustering. The centroids of each cluster serve as the final reduced scenarios, capturing both price and wind variability across 24 h. Their corresponding probability weights are also computed as the probability

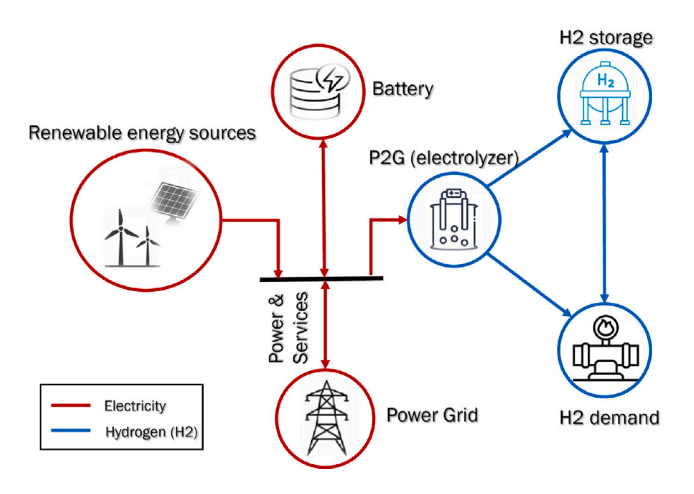


Fig. 2. Overview of the hybrid power plant structure modeled in EMERGE, including renewable generation, battery storage, and hydrogen conversion pathways.

of each scenario. This two-step framework, scenario generation via cGAN and reduction via clustering, ensures that the resulting set of scenarios is both statistically diverse and computationally tractable for use in day-ahead stochastic optimization models for HPPs.

3. Case study

To evaluate the effectiveness of the proposed cGAN-based scenario generation method, the generated wind power and electricity price scenarios are integrated into a stochastic optimization model developed within the EMERGE platform at TNO [15]. EMERGE enables comprehensive techno-economic modeling of hybrid energy systems by incorporating renewable generation alongside storage and conversion technologies. The system under study is a HPP consisting of wind turbines, PV solar generation, battery storage systems, and electrolyzer units capable of producing hydrogen. Fig. 2 shows the overall architecture of the modeled system. Red arrows represent electrical energy flows, while blue arrows indicate hydrogen flows. The optimization problem is formulated as a stochastic MILP. In the stochastic formulation, the cGAN-generated day-ahead scenarios for wind power and electricity prices are used to represent uncertainties in supply and market conditions. In contrast, the deterministic baseline uses only single-point forecast values, with no explicit treatment of uncertainty. The objective of the optimization is to minimize the total expected operational cost while maximizing revenue, subject to technical and operational constraints. Comparing the stochastic and deterministic configurations allows for assessing the value of uncertainty-aware planning in reducing imbalance costs and enhancing the scheduling of assets within the HPP.

The original MILP optimization model within the EMERGE platform [15] is formulated deterministically. In this study, the model is extended to a stochastic version to account for uncertainty in wind power and electricity market prices. To further enhance robustness against adverse scenarios, risk aversion is also incorporated using a Conditional Value-at-Risk (CVaR) formulation based on [29]. The general structure of the developed stochastic MILP model is summarized

$$\max (1 - \beta) \sum_{t \in \mathcal{T}} \operatorname{Profit}_t + \beta \cdot \left(\operatorname{CVaR}_{\alpha} - \frac{1}{1 - \alpha} \sum_{s \in S} p_s \cdot \Psi_s \right)$$
 (11)

$$Profit_t = Revenue_t - Cost_t, \quad \forall t$$
 (12)

$$Revenue_t = \sum_{s \in S} p_s \cdot \left(R_{t,s}^g + R_{t,s}^{h2} \right), \quad \forall t$$
 (13)

$$Cost_t = \sum_{s} p_s \cdot \left(C_{t,s}^g + C_{t,s}^b + C_{t,s}^{h2} \right), \quad \forall t$$
 (14)

$$R_{t,s}^{g} = P_{t}^{\exp} \cdot \lambda_{t,s}, \quad C_{t,s}^{g} = P_{t}^{\exp} \cdot \lambda_{t,s}, \quad \forall t, s$$
 (15)

$$R_{t,s}^{h2} = H_{t,s}^{deliv} \cdot \lambda_t^{h2}, \quad C_{t,s}^{h2} = Z_{t,s}^{su} \cdot c^{su} + H_{t,s}^{p} \cdot c^{h2}, \quad \forall t, s$$
 (16)

$$C_{t,s}^{\mathbf{b}} = \left(P_{t,s}^{\mathbf{b},\mathbf{ch}} + P_{t,s}^{\mathbf{b},\mathbf{dis}}\right) \cdot c^{\mathbf{b}}, \quad \forall t, s$$
 (17)

s.t.
$$P_{t,s}^{W} + P_{t,s}^{PV} + P_{t,s}^{b,dis} + P_{t}^{imp} = P_{t}^{exp} + P_{t,s}^{b,ch} + P_{t,s}^{e} + P_{t,s}^{com}, \quad \forall t, s$$
 (18)

$$P_{t,s}^{\mathsf{w}} = S_{t,s}^{\mathsf{w}} \cdot P_{t,s}^{\mathsf{w},\mathsf{scn}} \cdot P^{\mathsf{w},\mathsf{max}}, \quad P_{t,s}^{\mathsf{pv}} = S_{t,s}^{\mathsf{pv}} \cdot P_{t,s}^{\mathsf{pv},\mathsf{scn}} \cdot P^{\mathsf{pv},\mathsf{max}}, \quad \forall t, s$$
(19)

$$P_{t}^{e} = S_{t}^{h2} \cdot P^{h2,max}, \quad P_{t}^{com} = S_{t}^{com} \cdot P^{com,max}, \quad \forall t, s$$
 (20)

$$\begin{split} &P^{\mathrm{e}}_{t,s} = S^{\mathrm{h2}}_{t,s} \cdot P^{\mathrm{h2,max}}, \quad P^{\mathrm{com}}_{t,s} = S^{\mathrm{com}}_{t,s} \cdot P^{\mathrm{com,max}}, \quad \forall t, s \\ &\eta^{\mathrm{ch}} \cdot P^{\mathrm{b,ch}}_{t,s} \leq S^{\mathrm{b,ch}}_{t,s} \cdot P^{\mathrm{b,max}}, \quad \frac{1}{\eta^{\mathrm{dis}}} \cdot P^{\mathrm{b,dis}}_{t,s} \leq S^{\mathrm{b,dis}}_{t,s} \cdot P^{\mathrm{b,max}}, \quad \forall t, s \end{split}$$

(21)

$$P_{t,s}^{\text{b,ch}} \le M \cdot U_{t,s}^{\text{b}}, \quad P_{t,s}^{\text{b,dis}} \le M \cdot (1 - U_{t,s}^{\text{b}}), \quad \forall t, s$$
 (22)

$$SOC_{t,s}^{b} = SOC_{t-1,s}^{b} + \left(\eta^{\text{ch}} \cdot P_{t,s}^{\text{b,ch}} - \frac{1}{\eta^{\text{dis}}} \cdot P_{t,s}^{\text{b,dis}}\right), \quad \forall t > 1, s \quad (23)$$

$$SOC_{t-0,s}^{b} = SOC^{\text{init}}, \quad \forall s$$
 (24)

$$P_{t}^{\text{imp}} \leq M \cdot U_{t}^{g} \cdot P^{g,\text{max}}, \quad P_{t}^{\text{exp}} \leq M \cdot (1 - U_{t}^{g}) \cdot P^{g,\text{max}}, \quad \forall t \quad (25)$$

CVaR constraint:
$$CVaR_{\alpha} - \Pi_{s} \le \Psi_{s}$$
, $\forall s$ (26)

$$\Pi_{s} = \sum_{t \in \mathcal{T}} \left(R_{t,s}^{g} + R_{t,s}^{h2} - C_{t,s}^{g} - C_{t,s}^{b} - C_{t,s}^{h2} \right), \quad \forall s$$
 (27)

The objective function is defined in Eqs. (11) to (17), followed by the technical and operational constraints detailed in Eqs. (18) through (27). The detailed formulations of the hydrogen electrolyzer constraints and variables (e.g., $H_{t,s}^{\text{deliv}}$, $Z_{t,s}^{\text{su}}$, $H_{t,s}^{\text{p}}$, $P_{t,s}^{\text{e}}$, and $P_{t,s}^{\text{com}}$), as used in (16), (18), and (20), follow the modeling structure introduced in [30]. In that reference, the variables H^{deliv} , H^{p} , and P^{com} correspond to d, h, and P^{c} , respectively. The hydrogen electrolyzer model in this work is based on equations (8) to (25) of [30]. Note that the formulations defined in (21) to (24) are based on the battery storage model presented in [31]. The CVaR-based formulation follows the risk modeling approach in [29].

4. Numerical results

To assess the quality of the generated day-ahead scenarios, we present a representative case study comparing the synthetic outputs of the trained cGAN model against actual realizations and forecasted values. Fig. 3 illustrates the generated scenarios for electricity market prices (top) and wind power (bottom) for a sample test day (the last day, i.e., December 31, 2024). A total of 100 scenarios are generated and subsequently reduced to 10 representative scenarios for wind power $P_{t,s}^{\text{w,scn}}$ and electricity market prices $\lambda_{t,s}$ with a probability p_s . The shaded regions represent the 10th-90th percentile range of the generated scenarios, the dashed lines denote the scenario medians, and the solid lines show the real and forecasted data. The results demonstrate that the cGAN-generated scenarios more accurately capture the temporal trends and variability observed in the real data compared to the deterministic forecasts. This illustrates the model effectiveness in producing diverse and realistic samples suitable for uncertaintyaware decision-making. Note that $P_{t,s}^{\text{pv,scn}}$ is treated as deterministic and identical across scenarios, based on solar generation forecasts. The underlying dataset includes historical time-series data for wind generation, wind generation forecast, market prices, market price forecasts, load forecast, and solar generation forecast for the Netherlands spanning 2021-2024. These data were extracted from the ENTSO-E Energy Charts platform [32].

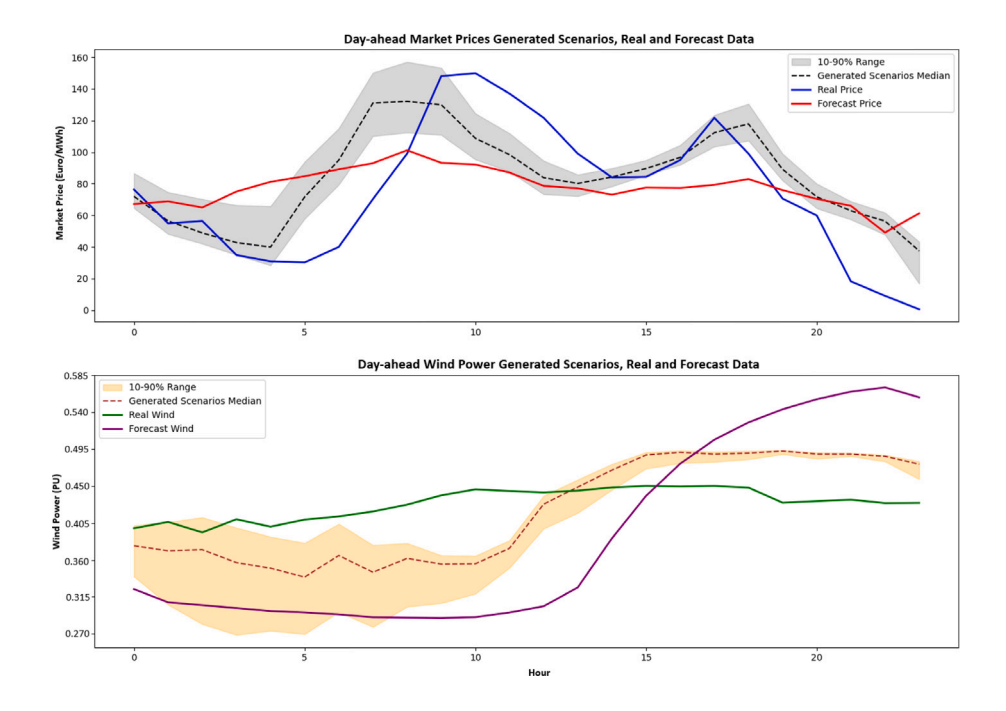


Fig. 3. Generated cGAN day-ahead scenarios (Median and 10%–90% Range) compared with forecasted and real values for market price (top) and wind power (bottom).

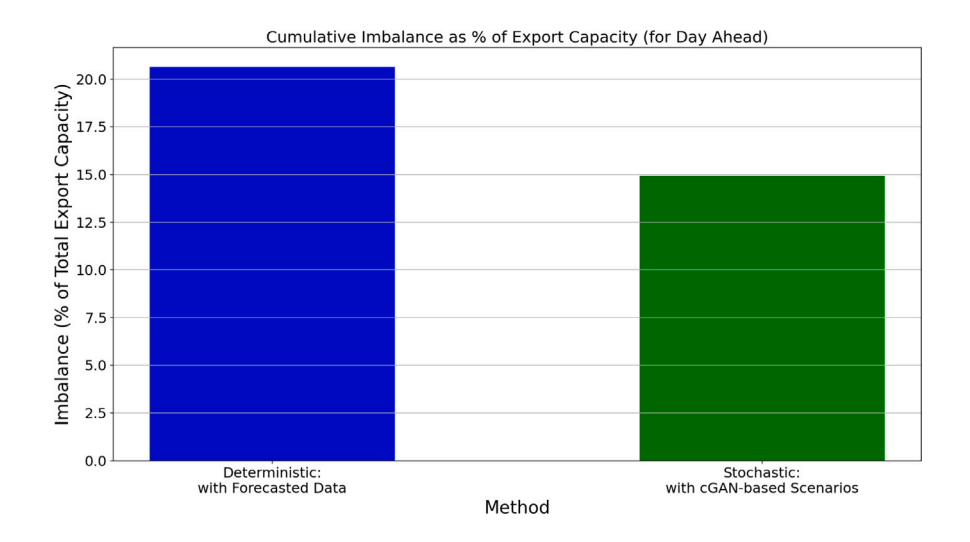


Fig. 4. Cumulative imbalance as percentage of total export capacity for day-ahead scheduling.

The generated scenarios are implemented in the stochastic version of the EMERGE platform, described in (11) to (27), to evaluate operational decision-making for a HPP. The modeled HPP includes 22 MW wind, 38 MW PV, a 6 MW/12 MWh battery energy storage system, a 6 MWe electrolyzer, and a 22 MW grid connection. The electrolyzer parameters and costs follow [30], and battery efficiency is set to 95%. For fair comparison with the deterministic case, a risk-neutral setting is adopted by setting the risk-aversion parameter $\beta=0$. To quantify the benefits of stochastic optimization, results from the scenario-based case (with cGAN-generated inputs) are compared to the deterministic case using only point forecasts. The imbalance is computed as the deviation between the real net power export and the net export optimized under forecasted or scenario-based inputs, normalized by total export

capacity:

$$Imb._{FOC} = \frac{|Net_{Real} - Net_{FOC}|}{P_{g,max}} \cdot 100$$

$$Imb._{SCN} = \frac{|Net_{Real} - Net_{SCN}|}{P_{g,max}} \cdot 100$$
where $Net = \sum_{t \in \mathcal{T}} \left(P_t^{exp} - P_t^{imp} \right)$ (28)

In (28), Net_{Real} refers to the net power calculated by the optimizer using actual realized data, Net_{FOC} is the net power obtained using forecasted input values, and Net_{SCN} denotes the net power resulting from the scenario-based stochastic optimization using cGAN-generated inputs. The denominator $P_{g,max}$ represents the total grid capacity of

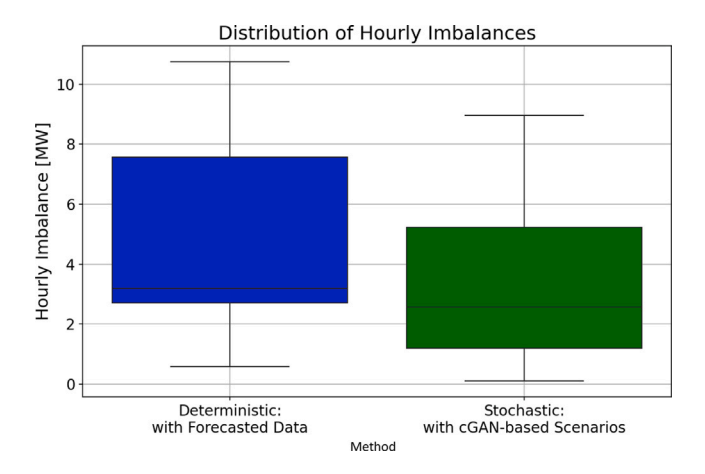


Fig. 5. Distribution of hourly imbalance values for deterministic and stochastic cases.

the HPP. The imbalance values are expressed as percentages of this capacity.

Fig. 4 illustrates the cumulative imbalance as a percentage of total export capacity for both cases based on (28). The stochastic optimization using cGAN scenarios achieves a lower imbalance level compared to the deterministic case (the imbalance costs is reduced from 20.63% to 14.94%). Additionally, Fig. 5 presents the distribution of hourly imbalances, highlighting that the stochastic approach reduces both the median and spread of imbalances.

Finally Fig. 6 illustrates the hourly profit dynamics with an emphasize on how the cGAN-based stochastic optimization approach outperforms the forecast-based deterministic baseline and closely tracks the profit realized under real observations. The total hourly profit is computed as the difference between the total hourly revenue, comprising electricity and hydrogen sales, and the total operational cost. This highlights the operational benefits of integrating realistic scenario modeling through the developed cGAN framework, improving the dispatch quality and economic performance of HPPs under uncertainty.

5. Conclusion

This paper proposed a conditional Generative Adversarial Network (cGAN)-based methodology for joint scenario generation of wind power and electricity market prices, with the goal of improving portfolio

management decisions for hybrid power plants (HPPs). The developed model was designed to capture both temporal dependencies and cross-feature correlations to address the limitations of traditional statistical and sampling-based approaches.

The generated scenarios were post-processed using clustering techniques to reduce dimensionality while preserving statistical characteristics. These reduced scenarios were integrated into a stochastic MILP model developed in the EMERGE platform at TNO to optimize HPP operations under uncertainty. Numerical experiments using Dutch data from 2021-2024 demonstrated that the developed cGAN-based stochastic approach achieved superior performance compared to a deterministic baseline using only point forecasts. In particular, it led to a reduction in cumulative imbalance, improved alignment with realtime market conditions, and better operational scheduling of storage and conversion assets within a HPP. Future work will aim to narrow the current performance gap by integrating additional uncertainty sources (e.g., solar variability and electrolyzer efficiency), extending the cGAN framework to multivariate spatial forecasting, enhancing input forecast accuracy, and incorporating online learning for adaptive scenario undates.

Declaration of competing interest

The authors declare the following financial interests/personal relationships which may be considered as potential competing interests: Mojtaba Moradi-Sepahvand reports financial support was provided by TNO Energy and Materials Transition. If there are other authors, they declare that they have no known competing financial interests or personal relationships that could have appeared to influence the work reported in this paper.

Acknowledgment

The author would like to thank the Wind Energy Department, Energy and Materials Transition Unit, The Netherlands at TNO for their support and resources that enabled this research.

Data availability

Data will be made available on request.

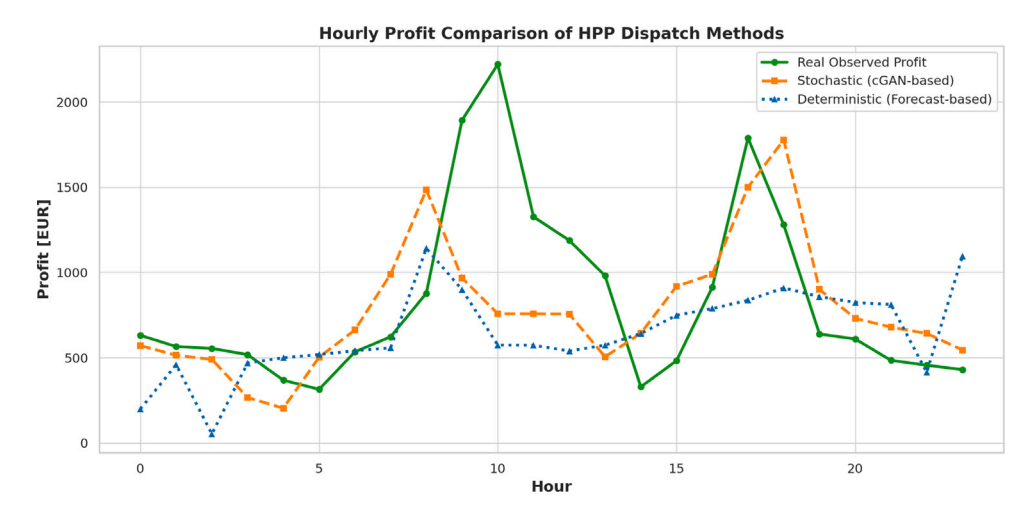


Fig. 6. Hourly profit comparison: Real observations vs. Stochastic dispatch (cGAN-based) vs. Forecast-based deterministic dispatch.

References

- [1] A. Zakaria, Firas B. Ismail, M.S. Hossain Lipu, Mahammad Abdul Hannan, Uncertainty models for stochastic optimization in renewable energy applications, Renew. Energy 145 (2020) 1543–1571.
- [2] Simeon Hagspiel, Antonis Papaemannouil, Matthias Schmid, Göran Andersson, Copula-based modeling of stochastic wind power in europe and implications for the swiss power grid, Appl. Energy 96 (2012) 33–44.
- [3] Daniel Villanueva, Andrés Feijóo, José Luis Pazos, Simulation of correlated wind speed data for economic dispatch evaluation, IEEE Trans. Sustain. Energy 3 (1) (2011) 142–149
- [4] Juan M. Morales, Roberto Minguez, Antonio J. Conejo, A methodology to generate statistically dependent wind speed scenarios, Appl. Energy 87 (3) (2010) 843–855.
- [5] Xi-Yuan Ma, Yuan-Zhang Sun, Hua-Liang Fang, Scenario generation of wind power based on statistical uncertainty and variability, IEEE Trans. Sustain. Energy 4 (4) (2013) 894–904.
- [6] Yize Chen, Yishen Wang, Daniel Kirschen, Baosen Zhang, Model-free renewable scenario generation using generative adversarial networks, IEEE Trans. Power Syst. 33 (3) (2018) 3265–3275.
- [7] Congmei Jiang, Yongfang Mao, Yi Chai, Mingbiao Yu, Songbing Tao, Scenario generation for wind power using improved generative adversarial networks, IEEE Access 6 (2018) 62193–62203.
- [8] Hu Wei, Zhang Hongxuan, Dong Yu, Wang Yiting, Dong Ling, Xiao Ming, Short-term optimal operation of hydro-wind-solar hybrid system with improved generative adversarial networks, Appl. Energy 250 (2019) 389–403.
- [9] Y. Wang, et al., Wind power scenario generation using conditional GANs, IEEE Trans. Sustain. Energy 12 (2) (2021) 1112–1121.
- [10] H. Liu, F. Liu, Deep generative modeling for energy systems forecasting, Appl. Energy 275 (2020) 115390.
- [11] Lin Ye, Yishu Peng, Yilin Li, Zhuo Li, A novel informer-time-series generative adversarial networks for day-ahead scenario generation of wind power, Appl. Energy 364 (2024) 123182.
- [12] Ran Yuan, Bo Wang, Zhixin Mao, Junzo Watada, Multi-objective wind power scenario forecasting based on PG-GAN, IEEE Trans. Power Syst. 38 (2) (2023) 1281–1293.
- [13] Z. Li, et al., Conditional style-based generative adversarial networks for renewable scenario generation, IEEE Trans. Sustain. Energy (2023).
- [14] Yubin Wang, et al., Operational scenario generation and forecasting for integrated energy systems, Appl. Energy 327 (2023) 120010.
- [15] Max Houwing, Nassir Cassamo, Edwin Wiggelinkhuizen, Energy Management System for Combined Renewable Generation, Storage and Conversion (EMERGE Model): Renewable Hybrid Power Plant Optimization, Technical Report TNO 2022 R10402, TNO, 2022.
- [16] Ashish Vaswani, Noam Shazeer, Niki Parmar, Jakob Uszkoreit, Llion Jones, Aidan N. Gomez, Łukasz Kaiser, Illia Polosukhin, Attention is all you need, Adv. Neural Inf. Process. Syst. 30 (2017).
- [17] Mary Phuong, Marcus Hutter, Formal algorithms for transformers, 2022.

- [18] Emma Yann Zhang, Adrian David Cheok, Zhigeng Pan, Jun Cai, Ying Yan, From turing to transformers: A comprehensive review and tutorial on the evolution and applications of generative transformer models, Sci 5 (4) (2023).
- [19] Philip B. Weerakody, Kok Wai Wong, Guanjin Wang, Wendell Ela, A review of irregular time series data handling with gated recurrent neural networks, Neurocomputing 441 (2021) 161–178.
- [20] Junyoung Chung, Caglar Gulcehre, KyungHyun Cho, Yoshua Bengio, Empirical evaluation of gated recurrent neural networks on sequence modeling, 2014.
- [21] M.D. Mujahid İrfan, R. Supriya, P. Malleswara Reddy, Haider Alabdeli, Sasikumar Gurumoorthy, Bi-directional gated recurrent unit approach for detecting and classifying high impedance fault in power distribution, in: 2024 Third International Conference on Distributed Computing and Electrical Circuits and Electronics, ICDCECE, IEEE, 2024, pp. 1–5.
- [22] Mohamed Reyad, Amany M. Sarhan, Mohammad Arafa, A modified adam algorithm for deep neural network optimization, Neural Comput. Appl. 35 (23) (2023) 17095–17112.
- [23] Qian Zhou, Bo Sun, A Gaussian-based WGAN-GP oversampling approach for solving the class imbalance problem, Int. J. Appl. Math. Comput. Sci. 34 (2) (2024).
- [24] Ishaan Gulrajani, Faruk Ahmed, Martin Arjovsky, Vincent Dumoulin, Aaron C. Courville, Improved training of wasserstein gans, Adv. Neural Inf. Process. Syst. 30 (2017).
- [25] Takuya Akiba, Shotaro Sano, Toshihiko Yanase, Takeru Ohta, Masanori Koyama, Optuna: A next-generation hyperparameter optimization framework, in: Proceedings of the 25th ACM SIGKDD International Conference on Knowledge Discovery & Data Mining, 2019, pp. 2623–2631.
- [26] Timothy O. Hodson, Root mean square error (RMSE) or mean absolute error (MAE): When to use them or not, Geosci. Model. Dev. Discuss. 2022 (2022) 1–10.
- [27] Alireza Ghasempour, Support Vector Regression to Predict Power Consumption, Technical Report, The University of New Mexico, 2024.
- 28] Gordon Anderson, Oliver Linton, Yoon-Jae Whang, Nonparametric estimation and inference about the overlap of two distributions, J. Econometrics 171 (1) (2012) 1–23
- [29] Farzin Ghasemi-Olanlari, Mojtaba Moradi-Sepahvand, Turaj Amraee, Two-stage risk-constrained stochastic optimal bidding strategy of virtual power plant considering distributed generation outage, IET Gener. Transm. Distrib. 17 (8) (2023) 1884–1901.
- [30] Manuel Tobias Baumhof, Enrica Raheli, Andrea Gloppen Johnsen, Jalal Kazempour, Optimization of hybrid power plants: When is a detailed electrolyzer model necessary? in: 2023 IEEE Belgrade PowerTech, IEEE, 2023, pp. 1–10.
- [31] Mojtaba Moradi-Sepahvand, Turaj Amraee, Secure expansion of energy storage and transmission lines considering bundling option under renewable penetration, Appl. Energy 347 (2023) 121414.
- [32] Energy Charts The Netherlands, Energy charts based on ENTSOE transparency platform, 2024, https://energy-charts.info/index.html?l=en&c=NL. (Accessed 2024).